Zero to π transition in superconductor-ferromagnet-superconductor junctions

J. W. A. Robinson,[1] S. Piano,[1,2] G. Burnell,[3] C. Bell,[4] and M. G. Blamire[1]
[1]*Department of Material Science, University of Cambridge, Pembroke Street, Cambridge CB2 3QZ, United Kingdom*
[2]*Physics Department, CNR-Supermat Laboratory, University of Salerno, 84081 Baronissi (SA), Italy*
[3]*School of Physics and Astronomy, E.C. Stoner Laboratory, University of Leeds, Leeds LS2 9JT, United Kingdom*
[4]*Kamerlingh Onnes Laboratory, Leiden University, P.O. Box 9504, 2300 RA Leiden, The Netherlands*
(Received 24 April 2007; revised manuscript received 7 August 2007; published 28 September 2007)

We report a systematic study of Nb/ferromagnet (FM)/Nb trilayer structures in which the FM layer is one of the strong ferromagnets Co, Fe, Ni, and $Ni_{80}Fe_{20}$(Py). Accurate control of the FM layer thickness has enabled detailed studies of the magnetic and transport properties in the superconducting state. In all cases, we estimate the thickness of the magnetic dead layer and the exchange energies of the ferromagnetic layers; in doing so, we demonstrate inconsistencies between the exchange energies derived elsewhere from superconductor (S)/FM bilayer experiments and from S/FM/S junction measurements compared to their bulk Curie temperatures, which may hint at further complexity in the underlying physics. We show results in support of a recent publication [J. W. A Robinson *et al.*, Phys. Rev. Lett. **97**, 177003 (2006)], focus in detail on a single 0-π phase transition, and show evidence for the appearance of a second harmonic in the current-phase relation at the minimum of the critical current.

DOI: 10.1103/PhysRevB.76.094522 PACS number(s): 74.45.+c, 74.50.+r, 74.20.Rp, 74.72.−h

I. INTRODUCTION

The proximity effect in superconductor/ferromagnet (S/FM) and S/FM/S structures leads to many interesting and peculiar effects that have been extensively studied in recent years,[1–4] both theoretically and experimentally. Advances in the fabrication of S/FM/S devices have opened up the opportunity to explore the physics of the π junctions predicted by Bulaevskii *et al.*,[5] for the case of tunnel barriers and by Buzdin[2] in diffusive systems; Buzdin predicted that under certain conditions the Josephson critical current I_c in a S/FM/S junction would change sign from positive to negative corresponding to a phase shift of π in the Josephson ground state and a damped oscillatory dependence of the singlet pair wave function in the FM layer. The underlying physics of the oscillating singlet pair wave function is similar to order parameter modulations described by the Larkin and Ovchinnokov state[6] and by the Fulde and Ferrell state;[7] as the singlet pair penetrates the FM layer, the two electrons of opposite spin experience an effective Zeeman field due to an exchange energy E_{ex}. This results in Zeeman splitting, a shift in the singlet pair momentum space, and an oscillating superconducting order parameter[2] of period ξ_1. Theses oscillations are exponentially decayed over the ferromagnetic coherence length ξ_2 according to $\sqrt{hD/E_{ex}(T)}$, with D as the diffusion constant of the ferromagnet and T as the temperature. For weak ferromagnetic metals, $E_{ex} \sim k_B T_c$, where T_c is the superconducting critical temperature; oscillations in the order parameter occur as a function of both T and d_F. However, for strong ferromagnetic metals, $E_{ex}(k_B T_\Theta) \gg k_B T_c$, where T_Θ is the Curie temperature of the ferromagnet; oscillations in the order parameter occur with d_F only,[9,8] but angstrom control of the thickness is required. Experimentally, oscillations in the order parameter can be seen as oscillations in I_c or characteristic voltage $I_c R_N$ (R_N is the normal state resistance).

One of the promises of the π-shift effect is the eventual implementation of this physics into quantum computing where information is stored in two-level quantum systems, or qubits. Many theoretical and experimental advances have been achieved toward the physical realization of solid-state qubit systems,[10,11] with particular breakthroughs being made in those systems incorporating π-shift physics. However, all S/FM systems investigated so far present a number of physical challenges to their reproducibility and understanding, particularly, a maximization of $I_c R_N$ in the π state, control of the magnetically "dead" region in the ferromagnetic barrier which corresponds to a fraction of the ferromagnetic which exhibits a zero-net moment,[12–15] and inconsistences in experimentally derived E_{ex} values from S/FM bilayer experiments and from S/FM/S junction measurements compared to their bulk T_Θ.

In this paper, we report a systematic study of S/FM/S thin-film structures consisting of Nb leads and strongly ferromagnetic barrier metals: Co, Ni, Fe, and $Ni_{80}Fe_{20}$(Py). In particular, we show details of the magnetic properties of these thin films and their transport properties in current perpendicular to plane devices in the superconducting state. The results are divided into four sections: Section III addresses aspects of a magnetic dead layer where its scale is estimated in all of the ferromagnets studied; in Sec. IV, we show results to support a recent publication (Ref. 15) which reported multiple oscillations between 0 and π states; in Sec. IV, we have identified an interesting inconsistency between experimentally derived exchange energies in S/FM bilayer experiments and from S/FM/S junction measurements; Sec. IV reports a single phase transition from 0 to π in Nb/Co/Nb junctions and provides evidence for a second harmonic in the current-phase relation.

II. EXPERIMENTAL METHODS

Thin films of Nb/Co/Nb, Nb/Py/Nb, Nb/Ni/Nb, and Nb/Fe/Nb were prepared on thermally oxidized (100) Si substrates with a 250 nm oxide layer on the surface in an

TABLE I. Deposition parameters for all metals grown by dc magnetron sputtering for this study.

Target metal	Deposition rate at 1 rpm (nm)	Power (W)	Speed range (rpm)	Thickness (±0.2 nm)
Nb	6.89	90	028	250
Cu	4.39	30	0.22	20
Ni	2.12	40	0.20–4.2	0.5–10.5
Co	1.18	40	0.36–3.6	0.5–5.0
Py	1.64	40	0.33–3.3	0.5–5.0
Fe	2.0	40	0.22–2.2	0.5–5.0

ultrahigh vacuum deposition chamber. For device fabrication, films were deposited on 10×5 mm^2 chips. For magnetic characterization in a vibrating sample magnetometer (VSM), films were grown simultaneously on 16–25 mm^2 chips. Chip dimensions were measured to an accuracy of ±0.1 mm using vernier calipers. Before loading the chips into the deposition chamber, they were cleaned in acetone in an ultrasound bath for 30 min and subsequently dried with a nitrogen air gun with acetone and, finally, isopropanol. All of the films were grown by dc magnetron sputtering in an Ar plasma pressure of 1.5±0.01 Pa, where a minimum film stress is expected. Prior to the depositions, the chamber was baked out for 7 h and subsequently cooled with liquid nitrogen via a liquid nitrogen jacket for 2 h; the deposition chamber had a base pressure of better than 5×10^{-6} Pa and an oxygen partial pressure of $<3\times10^{-9}$ Pa, as confirmed by an *in situ* residual gas analyzer.

The films were grown in one run without breaking vacuum. In a single run, multiple chips were placed on a rotating holder which passed, in turn, under three magnetrons: Nb, Cu, and the FM target (Fe, Co, Py, or Ni). The speed of rotation was controlled by a computer operated stepper motor with a precision angle of better than 3.6°, and each sample was separated by an angle of at least 10°. Deposition rates for each target were calibrated in separate depositions using atomic force microscopy and a photolithographic lift-off technique (see Table I for a summary of the deposition parameters for all target materials). For the ferromagnet barrier metals, their deposition rates and, hence, their thickness d_F were varied by controlling the chip's angular speed as it passed under the respective target while maintaining a constant power to the magnetron and a constant plasma pressure. This was achieved from a knowledge of the chip's position relative to the target material, θ, and by programming the rotating flange speed to give a linear variation of d_F with θ so that $d(d_F/d\theta)=$const. d_F is inversely proportional to the instantaneous speed of deposition at time t (seconds) so that $d_F\propto1/V_t$. Hence, it can be shown that to achieve a linear variation of d_F with θ, one programs the speed at θ and t, $V(\theta)_t$, of the deposition according to

$$V_F\propto\frac{V_iV_f}{V_f-V_i}\left(\frac{V_iV_f}{V_f-V_i}-\frac{\theta}{2\pi}\right)^{-1}, \quad (1)$$

where V_i and V_f are the initial and final chip speeds, respectively, in units of rpm. This method of varying d_F guaranteed, in all cases, that the interfaces between each layer were prepared under the same conditions while providing precise control of d_F. For Co, Fe, and Py, d_F varied from 0.5 to 5 nm while for Ni, d_F varied from 1.0 to 10 nm. A second set of Co barrier films (sample set 2) were grown so that details of a single phase transition of π could be measured; for this run, the Co barrier thickness varied from approximately 1.5 to 2.5 nm.

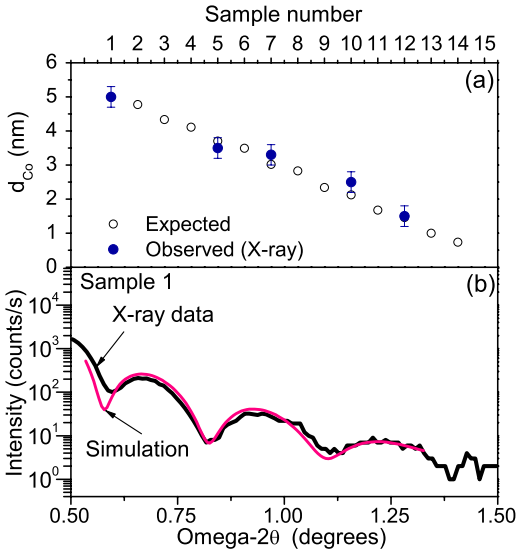

FIG. 1. (Color online) Low angle x-ray reflectivity data from a set of Nb(5 nm)/Co(d_{Co})/Nb(5 nm) samples: (a) Co thickness versus sample number where the solid (blue) and hollow (black) circles represent the measured (observed) Co thickness, by comparing the Kiessig fringes to a simulation and the expected Co thickness, respectively; (b) experimental (black) and simulated Kiessig fringes (pink) for sample 1 where the expected Co thickness was 5 nm and the observed Co barrier thickness from the simulation is 5±0.2 nm.

The quality of the Nb for all the runs was confirmed by an average T_c of 9.0±0.05 K from a measurement of electrical resistance versus temperature using a van der Pauw wiring configuration and an average residual resistance ratio of RRR$=R(300K)/R(4.2K)=4.2$.

To confirm control over the variation in d_F, we performed low angle x-ray reflectivity measurements of a set of Nb/Co/Nb thin films, where the top and bottom Nb had a thickness of 5 nm while the Co thickness was varied from 0.5 to 5.0 nm. A series of low angle x-ray scans was made, and the observed Co thickness was extracted by fitting the period of the Kiessig fringes to a simulation. It was found that our expected Co thickness was well correlated with the observed Co thickness with a mean deviation of ±0.2 nm. Figures 1(a) and 1(b) show (a) a comparison of the observed Co thickness with the expected Co thickness and (b) an example of low angle x-ray data plotted with the equivalent simulation data for the same Co and Nb layer thicknesses.

Films were patterned using optical lithography followed by broad Ar ion milling (3 mA cm^{-2}, 500 V beam) to produce micron-scale tracks and millimeter-scale contact pads for wire bonding to chip carriers. The tracks were then patterned with a Ga^+ focused ion beam (FIB) microscope

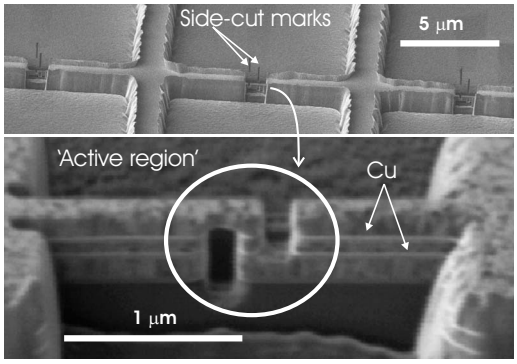

FIG. 2. Focused ion beam micrographs of an etched track: (top) three devices at 20° to the surface; (bottom) the active region of a device showing the Cu guides used to assist the side-cutting procedure.

(Philips/FEI FIB 200) to achieve vertical transport with a device area in the 0.2–1 μm^2 range. Details of the FIB processing can be found elsewhere.[16] Figure 2 shows two FIB micrographs: (a) an etched track showing three junctions with different cross-sectional areas with the line cuts, which arise from the side-cutting technique, labeled; (b) a micrograph of a typical junction. Because the ferromagnetic barrier metals have a similar secondary electron emission to the Nb electrodes, the contrast in the FIB microscope was poor, which made processing difficult. Consequently, the yield of functional devices was low. We overcame this problem by depositing a 20 nm thick layer of Cu sandwiched within 250 nm of Nb. Cu, having a higher secondary electron emission compared to Nb, improved the contrast considerably and served as a bright cutting guide, which increased our device yield to above 80%. The Cu was located 50 nm from the FM barrier, where 50 nm $> \xi_{Nb}$, and being only 20 nm thick implies that $d_{Cu} \ll \xi_{Cu}$. The Cu is, therefore, fully proximitized by the superconducting Nb and plays no part in the transport properties of the junctions.

Devices were wire bonded onto chip carriers so that transport characteristics could be measured using a four-point technique in a custom made liquid-He dip probe that included a microwave antenna, a heating stage, a Si diode thermometer with a temperature sensitivity of ±0.01 K, and a 120 mT solenoid. Samples were in good thermal contact with the thermometer. Current-voltage characteristics of the devices were made using a lock-in amplifier; the differential resistance $dV/dI(I)$ of a device was measured as a function of the applied bias current. From this measurement, I_c was extracted; I_c was defined as the point where $dV/dI(I)$ increased above the value for a high bias current and then proceeded to drop to the minimum resistance of the apparatus of 10 $\mu\Omega$. The noise floor of our apparatus is 100 nV, which, for a 1 μA bias, corresponds to 10 $\mu\Omega$. All of our devices have different cross-sectional areas. Hence, to normalize our data, we multiplied I_c by R_N to give the characteristic voltage I_cR_N. R_N was measured by applying a quasi-dc bias current of 3–5 mA, which enabled the nonlinear portion of the current-voltage curves to be neglected but was not large enough to drive the superconducting Nb electrodes into a normal resistive state. The I_c of the devices ranged from about 3 mA to below the minimum sensitivity of our apparatus (50 nA), while the R_N was in the range 0.5 mΩ to 0.5 Ω.

III. MAGNETIC DEAD LAYERS

As previously reported in Nb/FM/Nb films,[8,12] a substantial magnetic dead layer exists at the Nb/FM interface, while in systematic studies of thin ferromagnetic films,[17,18] the magnetic dead layer exists at the surface—even where oxidation is eliminated. The magnetic dead layer manifests itself as a loss in magnetic moment, and its scale depends on the ferromagnetic metal and whether it is a pure element or an alloy and on its temperature. In systems where the ferromagnetic thin film is relatively thick, the presence of a magnetic dead layer might be considered less important to the bulk properties; however, in thin-film stacks where the thickness of the ferromagnetic film approaches the total magnetic dead layer thickness (D), the presence of the magnetically inert region becomes increasingly important. In alloys, the dead layer can partly be explained by changes in alloy stoichiometry at the surface and/or interface, which give rise to different electronic structures and exchange interactions. For pure element ferromagnetic films, where intermixing is ruled out, the underlaying physics of a magnetic dead layer is very interesting but poorly understood. In the strong ferromagnet 3d transition metals of Fe, Co, and Ni, D is relatively small, being typically <1 nm at room temperature, and, therefore, its effect on the magnetic properties of bulk films is negligible. However, when the current is perpendicular to the interface, the presence of a magnetic dead layer cannot be neglected because it will modify the transport properties across the interface, which is true when the film is thick, $d_F \gg D$, and when $d_F \sim D$.

A number of factors can partly explain the presence of a magnetic dead layer: (1) lattice mismatch at the Nb/FM interface, leading to a reduction in the ferromagnetic density and a correspondingly disordered crystal structure at the interface,[19] which may be commensurate with a reduction in both the bulk exchange interaction and T_Θ (Refs. 20–23) (2) hybridization of ferromagnetic atoms with Nb. Such mixing will doubtlessly result in the formation of various magnetic and nonmagnetic alloys at the interface and possibly the inclusion of isolated Nb atoms deep inside the ferromagnet and vice versa. To begin understanding what a magnetic dead is in our films we have estimated D for all of the ferromagnets studied in this paper at room temperature by measuring the saturation moment per unit surface area as a function of d_F $[M_s/A(d_F)]$: $\approx$0.75 nm for Co, $\approx$0.5 nm for Py, and $\approx$1.75 nm for Ni, and 1.1 nm for Fe [see Fig. 3(a)]. Because for all of the ferromagnetic metals $d_F < 10$ nm, the diamagnetic slope present in the hysteresis loops from the Nb, substrate, and holder had to be carefully subtracted. The subtraction was made by growing a 500 nm Nb film on a Si/SiO_2 substrate and by measuring its diamagnetic slope using the same VSM parameters and conditions as those used to measure the Nb/FM/Nb films. These data were then subtracted from the original Nb/FM/Nb hysteresis loop data sets.

Besides deriving D from Fig. 3(a), it is also possible to estimate the bulk magnetization M_B of the barrier metals.

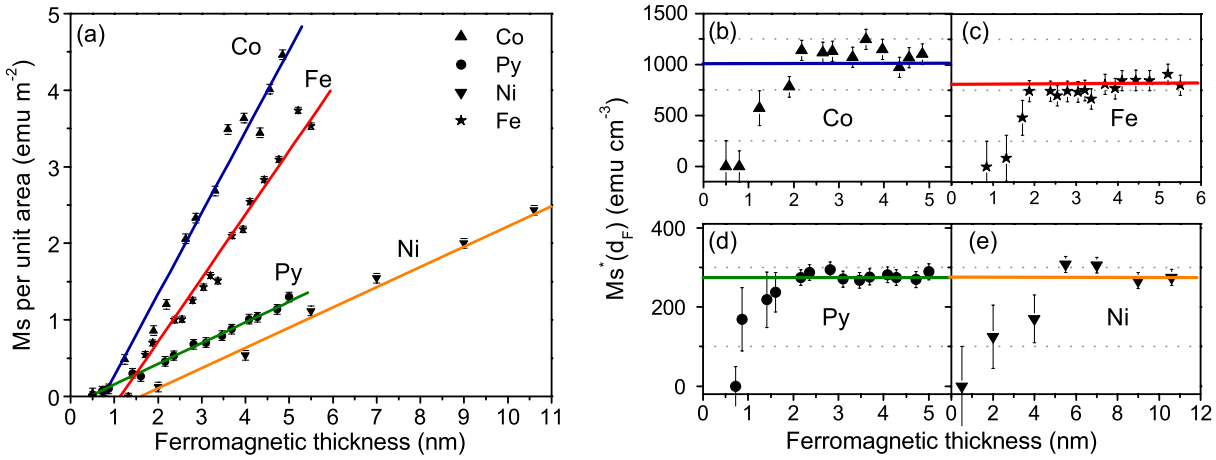

FIG. 3. (Color online) Room temperature magnetic data for Nb/FM/Nb films: (a) saturation magnetization (M_s) per unit surface area versus Co, Ni, Py, and Fe thicknesses; [(b)–(e)] saturation magnetization per unit active FM volume versus Co, Fe, Py, and Ni thicknesses, $M_s^*(d_F)$. Solid lines in (a) are least-squares fits and the horizontal solid lines in (b)–(e) correspond to the bulk magnetization.

Slater[24] and Pauling[25] showed that the exchange interaction is responsible for creating the imbalance of spin-up and spin-down states and that from a knowledge of a ferromagnet's electron band structure it is possible to predict the net magnetic moment per atom as a function of the number of $3d$ electrons/holes: $\simeq$1420 emu/cm^3 for Co, $\simeq$600 emu/cm^3 for Ni, $\simeq$520 emu/cm^3 for Py, and 2600 emu/cm^3 for Fe.[26] However, from Fig. 3(a), M_B is suppressed from these expected bulk values: $\simeq$1000 emu/cm^3 for Co, $\simeq$270 emu/cm^3 for Py, $\simeq$270 emu/cm^3 for Ni, and $\simeq$830 emu/cm^3 for Fe. The conclusion is that the magnetism in Nb/FM thin film systems is, in some way, weakened. From literature, we have found that such discrepancies in the measured slopes is generally accepted as fact; we have compared M_B of our films with earlier studies in the literature and have found that for Co and Ni, both their magnetic dead layers and their total moments for a given thickness greater than D are very close to those reported in systematic studies of Nb/FM multilayers.[13,14] D for Py is similar to studies on epitaxial Nb/Py thin films.[12]

To further understand the suppression in M_B in Co, Fe, Ni, and Py, we have calculated its value as a function of d_F. From this, the change in M_B from the onset of magnetism, at the edge of the magnetic dead layer, to where it reaches some bulk value is calculated. To achieve this, we have subtracted D from d_F to give the moment per unit active ferromagnetic volume only, $M_s^*(d_F)$,

$$M_s^*(d_F) = \frac{M_s f(d_F)}{A(d_F - D)}, \tag{2}$$

where A is the surface area of a chip. Figures 3(b)–3(e) summarize the results. We find that for Co, Fe, Ni, and Py, the moment at the higher thickness regimes reaches a plateau which corresponds to a suppressed bulk magnetization of the ferromagnetic film.

As d_F approaches the dead layer regime, the saturation magnetization is found to decrease gradually to a zero minimum, implying a mixing of magnetic moments and a zero-net magnetic moment. This may imply that a magnetic dead layer is a frozen spin state with zero order and that it may exhibit similar properties to a spin-glass material. We expect that the decrease in moment as $d_F \rightarrow D$ occurs by virtue of a Nb/FM alloy forming at the interface. This needs to be confirmed by transmission electron micrographs of the barrier layers. Pick *et al.*[22] extensively studied theoretically the effects of Nb nearest neighbors surrounding a variety of ferromagnetic atoms; they showed that the number of Nb nearest neighbors strongly affects the moment of ferromagnetic atoms and explains a suppression in M_B in terms of hybridization and a widening of the $3d$ band of the ferromagnet atoms. Similar experimental results were reported by Lee *et al.* in Cu/Ni/Cu films.[27] However, strongly correlative results are obtained by applying Eq. (2) to magnetic data on Nb/Co bilayers reported by Obi *et al.*[13] In this case, we find that the saturation magnetization reaches a bulk value of only 1100 emu/cm^3, a value very close to the one we report, 1000 emu/cm^3.

Liebermann *et al.* first reported a ferromagnetic dead layer in Fe thin films[28] and then in Ni and Co films[29] by growing atomic layers by electrodeposition on single crystal noble metal substrates in the presence of a magnetic field. They demonstrated a loss in magnetic moment at the surface without diffusion of substrate atoms into the ferromagnetic layers and vice versa. Their theoretical studies suggested that a loss in surface moment in pure elemental ferromagnets is likely to be owed to a reduction in the number of d holes in the surface atoms. Their results also suggest that the presence of a capping layer does not contribute to a further reduction of the exchange interaction; however, more recent studies on Ni/Cu (Ref. 18) and Co/Cu (Ref. 17) films grown by sputter deposition have shown that T_Θ can be manipulated by growth temperature and by a Cu-capping layer. This observed difference might be due to the fact that sputter deposition is a highly kinetic process compared to electrodeposition, which is well known to result in the formation of atomic pores/defects/intermixing at interfaces by virtue of

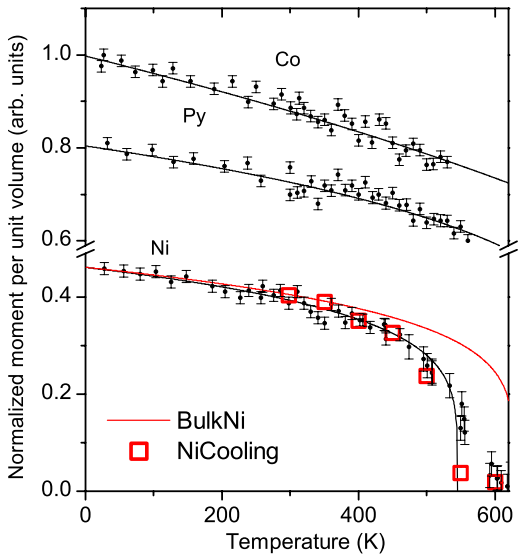

FIG. 4. (Color online) Thermal (warming) variation of the bulk magnetization (normalized) for Co, Py, and Ni (black dots) and theoretical fits (solid black curves) for T_Θ values of 1200 K for Co, 800 K for Py, and 571 K for Ni; the expected bulk Ni curve (solid red) for T_Θ of 640 K. Hollow red squares are cooling data for Ni only.

momentum transfer as sputtered fragments bombard the surface. In their pioneering paper on magnetic dead layers, Liebermann *et al.* developed a simple model for the surface of a ferromagnetic film. By assuming a parabolic band and that all spins in the 3*d* band are completely aligned at 0 K, they showed that for a film of N atomic layers the reduced spontaneous magnetization M_{sp} is

$$\frac{M_B(T)}{M_B(0)} = \left[\frac{N-2D(T)}{N-2D_0}\right]\frac{M_T(T)}{M_T(0)}, \tag{3}$$

where $M_T(T)/M_T(0)$ is taken to be the ratio of the true bulk Ni magnetization for $T<T_\Theta$ to the bulk magnetization at 0 K so that deviations of $M_B(T)/M_B(0)$ from a bulk behavior are due to a true magnetic dead layer effect and not due to deviations of the bulk Stoner magnetizations. We have measured the thermal variation of the saturation magnetization, $M_B(T)$, of Co, Ni, and Py when sandwiched between thick Nb layers. To be certain, $M_B(T)$ with temperature was not weakened by a thermally activated diffusion of ferromagnetic atoms into Nb, or vice versa; at the interface we measured both the magnetization when warming and cooling. The warming and cooling data agreed for all three barrier systems up to a temperature of 620 K. Above this temperature, M_s was found to drop by virtue of thermally activated diffusion. We have modeled the warming and cooling data of $M_s(10<T<620\ \mathrm{K})$ with the generic equation $M_B(T)/M_B(0)=(1-T/T_\Theta)^\beta$, where $M_s(0)$ is the saturation magnetization at absolute 0 K, T is the measuring temperature, and β and T_Θ are fitting parameters. This gives T_Θ values of 1200 K for Co, 571 K for Ni, and 800 K for Py (Fig. 4). Data for Ni are the most reliable because we have a full data set. For Ni, we have approximated D at 4.2 K by estimating its scale at 0 K by applying Eq. (3) to the data in Fig. 4. Assuming that $D_{4.2\ \mathrm{K}}\approx D_0$, we input $D_T=D_{300\ \mathrm{K}}=1.5$ nm into Eq. (3), which gives $D_0\approx 1.3$ nm. The value 1.3 nm is larger than the one estimated by Liebermann *et al.*, 0.4 nm. However, this makes sense because in our metallic system, interdiffusion at the ferromagnetic surface cannot be ruled out because Ni is known to form a variety of magnetic and nonmagnetic alloys with Nb.[30] All of the magnetic data derived in this section are summarized in Table II.

IV. MULTIPLE PHASE TRANSITIONS

The characteristic voltage of a Josephson junction as a function of d_F is predicted theoretically[2] to oscillate where a number of parameters are used to derive $I_cR_N(d_F)$: (a) E_{ex}, (b) d_F, and (c) the electron mean free path ℓ, where ℓ determines the clean ($\ell>d_F$ and $\ell>\hbar v_f/E_{ex}$) and dirty limit ($\ell<d_F$ and $\ell<\hbar v_f/E_{ex}$) regimes. v_F is the Fermi velocity. For Co and Fe, the oscillations can be modeled entirely in the clean limit, in which case I_cR_N is modeled by Eqs. (4) (Ref. 31) and (5), respectively,

TABLE II. A summary of the magnetic data derived in this paper (†) and elsewhere. Symbol key: T_Θ, the Curie temperature; d_{bulk}, the distance into the ferromagnet to achieve bulk magnetization M_B; D, the magnetic dead layer thickness at 4.2 or 300 K, as marked.

Ferromagnetic metal	T_Θ [Fig. 3(a)] (K)	d_{bulk} (300 K) (nm)	M_B (Fig. 4) (emu/cm^3)	M_B (Ref. 24) (emu/cm^3)	Deviation %	D (4.2 K) (nm)	D (300 K) (nm)	Ref.
Nb/FM/Nb								
Py	800±50	2.5±0.5	270	520	−48		0.5	†
Py			680	520	+31			10
Ni	571±10	6.0±1.0	270	600	−55	1.3	1.5	†
Co	1200±50	2.5±0.3	1000	1420	−30		0.8	†
Fe		2.0±0.3	830	260	−68		1.1	†
Nb/FM								
Co		1.5±0.2	1100	1420	−23		0.7	11

TABLE III. A summary of the parameters used to model all of the transport data presented in this section.

Ferromagnetic barrier metal	ξ_1 (nm)	ξ_2 (nm)	ν_F (ms^{-1})	E_{ex} (meV)	Δ (meV)	ℓ (nm)
$Ni_{80}Fe_{20}$	1.4	0.46	2.2×10^5	201	1.3	2.3±0.4
Ni	4.1	1.2	2.8×10^5	80	1.3	7.0±0.5
Co	3.0	0.3	2.8×10^5	309	1.3	>5.0
Fe	3.8	0.25	1.98×10^5	256	1.3	>5.0

$$I_cR_N \propto \frac{|\sin(2E_{ex}d_F/\hbar\nu_f)|}{2E_{ex}d_F/\hbar\nu_f}, \tag{4}$$

$$I_cR_N(d_F) = I_cR_N(d_0)\left|\frac{\sin\dfrac{d_F-d_1}{\xi_2}}{\sin\dfrac{d_1-d_0}{\xi_2}}\right|\exp\left\{\frac{d_0-d_F}{\xi_1}\right\}, \tag{5}$$

where d_1 is the thickness of the ferromagnet corresponding to the first minimum and $I_cR_N(d_0)$ is the first experimental value of I_cR_N. The decay envelope determining the modulation amplitude is given by ξ_1 and can be much longer than the oscillation period ξ_2; for Co, $\xi_1 \simeq 3.0$ nm and $\xi_2 \simeq 0.3$ nm. For Eq. (4), the only fitting factor, besides the numerical prefactor, was E_{ex}.

For Ni and Py, the oscillations exist in both the clean and dirty regimes; hence, the data have been modeled using two theories: Eq. (4) and a theory that is only valid for a ferromagnetic metal in the diffusive limit with a strong E_{ex}, in which case the expression used is[32]

$$I_cR_N \propto \left|\mathrm{Re}\sum_{\omega_m>0}\frac{\Delta^2}{\Delta^2+\omega_m^2}\int_{-1}^{1}\frac{\mu}{\sinh(k_\omega d_F/\mu\ell)}d\mu\right|, \tag{6}$$

where Δ is the superconducting order parameter and ω_m is the Matsubara frequency given by $\omega_m=\pi Tk_B(2m+1)$, where T is the transmission coefficient and m is an integer number. $k_\omega=(1+2|\omega_m|\tau/\hbar)-2iE_{ex}\tau/\hbar$ and $\mu=\cos\theta$, where θ is the angle the momentum vector makes relative to the distance normal to the S/FM interface. ℓ is given by $\nu_f\tau$ and τ is the momentum relaxation time. To fit Eq. (6), suitable Fermi velocity, superconducting energy gap, and exchange interaction energy had to be chosen: For Py we assumed $\nu_f(\mathrm{Py})=2.2\times10^5$ ms^{-1} and an electron mean free path of $\ell_{\mathrm{Py}}\simeq 2.3$ nm, and for Ni we assumed $\nu_f(\mathrm{Ni})=2.8\times10^5$ ms^{-1} and an electron mean free path of $\ell_{\mathrm{Ni}}\simeq 7$ nm. The superconducting energy gap of Nb is $\Delta=1.3$ meV. A summary of all of the fitting parameters and derived material constants for Co, Fe, Ni, and Py from the oscillations and model fits is given in Table III.

$I_cR_N(d_F)$ for Co, Fe, Py, and Ni at 4.2 K is shown in Figs. 5(a), 5(c), 6(a), and 6(c), respectively. The error in d_F is estimated from x-ray reflectivity, as discussed in Sec. II, to be ±0.2 nm. We assume that the error in d_F is a systematic one. The principal sources of error in d_F arise from the following: (1) small variation in the Ar plasma pressure during the deposition and (2) small power and voltage variations during the deposition. The vertical error bars are derived from the measured variation in I_cR_N for a minimum of three junctions and a small noise contribution from the current source.

A clean limit behavior with multiple phase oscillations from 1 to 5 nm is exhibited by Co and Fe barrier devices only [Figs. 5(a) and 5(d)]. The long clean limits arise most obviously from the use of a pure element, but also from the vertical coherence likely[33] even in polycrystalline heterostructures. Further evidence of the oscillatory dependence of the characteristic voltage is given by measurements of its thermal variation; a set of I_cR_N vs temperature curves is given in Fig. 5(b) for Co devices and 5(d) for Fe devices. For Co, the characteristic voltage decreases to 0 V with increasing temperature in an approximately monotonic fashion; however, for Fe, the decay seems more complex. For Co, no critical current was seen for $T>8.1$ K although there was some reduction of the differential resistance around 0 V until $T\approx 8.5$ K. For $T>8.5$ K, an Ohmic behavior was observed. For Fe, the decline in characteristic voltage to 0 V with temperature depended on the junction measured. To ensure that this complexity was not an artifact of thermal drift, the data sets were repeated while taking the points in a random order. No thermal hysteresis was reported, and, in fact, approximately the same $I_cR_N(T)$ relation was recorded. Assuming that this complexity is real and assuming E_{ex} is too large in Fe for the standard temperature dependence of ξ_1 and ξ_2 to be important, one may speculate that some other mechanism besides temperature must be contributing to the depairing processes. One possible explanation is that the Fe barrier devices exhibit enhanced spin-flip scattering at the interface at temperatures approaching the superconducting critical temperature. Such scattering is known to have striking effects on ξ_1 and ξ_2.[35]

For Co, it is interesting to observe the relation between the rate in the decline of the characteristic voltage with temperature to 0 V for a given d_F; following the approach of Blum *et al.*,[34] we define the relative rate of decay, α_T, of $I_cR_N(T)/I_cR_N(4.2\ \mathrm{K})$ as

$$\alpha_T = \frac{d}{dT}\left[\ln\frac{I_cR_N(T_m)}{I_cR_N(4.2\ \mathrm{K})}\right]. \tag{7}$$

α_T a function of Co barrier thickness is plotted in Fig. 5(a). α_T oscillates in phase with the characteristic voltage. This relation seems commonsensical in the sense that when d_F corresponds to characteristic voltages near a transition, its

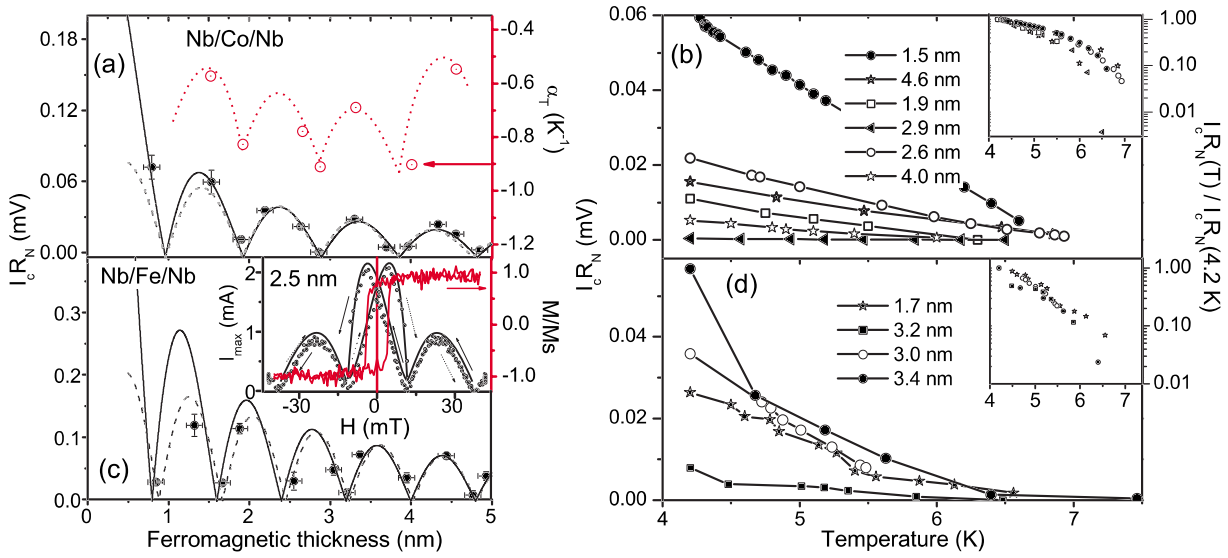

FIG. 5. (Color online) [(a) and (b)] Data for Co barrier devices: (a) I_cR_N and α_T versus barrier thickness at 4.2 K (red dotted line is an eye guide only). (b) I_cR_N versus temperature and the inset is $I_cR_N(T)/I_cR_N$ (4.2 K) versus temperature for various devices. [(c) and (d)] Data for Fe barrier devices: I_cR_N versus barrier thickness at 4.2 K and the inset is a typical Fraunhofer pattern for a device with a 2.5 nm thick Fe barrier. The central peak is offset by 4.9 mT, which corresponds to the coercive field of the Fe barrier, as confirmed by the (red) hysteresis loop. (d) I_cR_N versus temperature for various devices and the inset is $I_cR_N(T)/I_cR_N$ (4.2 K) versus temperature. The black solid and dashed curves in (a) and (c) are fits to Eqs. (4) and (5), respectively.

rate of decay to 0 V with increasing temperature is appreciably slower than for those devices where the characteristic voltage is large for a given d_F. Similar results were reported by Blum *et al.*[34]

For Py and Ni, the characteristic voltage oscillations span through both the clean and dirty regimes [see Figs. 6(a) and 6(c)]. In the clean regime, the characteristic voltage is maximized, which is implied by the fact that the datum points fit the clean limit theory, but where the data fall below the clean limit the characteristic voltage is suppressed; the data are accurately modeled by Eq. (6). The crossover from clean to dirty in Ni and Py is understood by virtue of their electron mean free paths being short. In Py, a short electron mean free path is well understood; by photoemission spectra experiments, it is found that large scattering potentials of the minority electron spin states exist at Fe impurity sites.[36] From theoretical fits, we can estimate that 1.5 nm$<\ell$(Py)$<$2.5 nm, which is close to other reported values for $Ni_{80}Fe_{20}$.[37] For Ni, the short electron mean free path is probably due to the inclusion of impurities and interdiffusion of Ni and Nb at the interface; the solubility of Nb into Ni has been thoroughly characterized by Chen *et al.*,[30] where it has

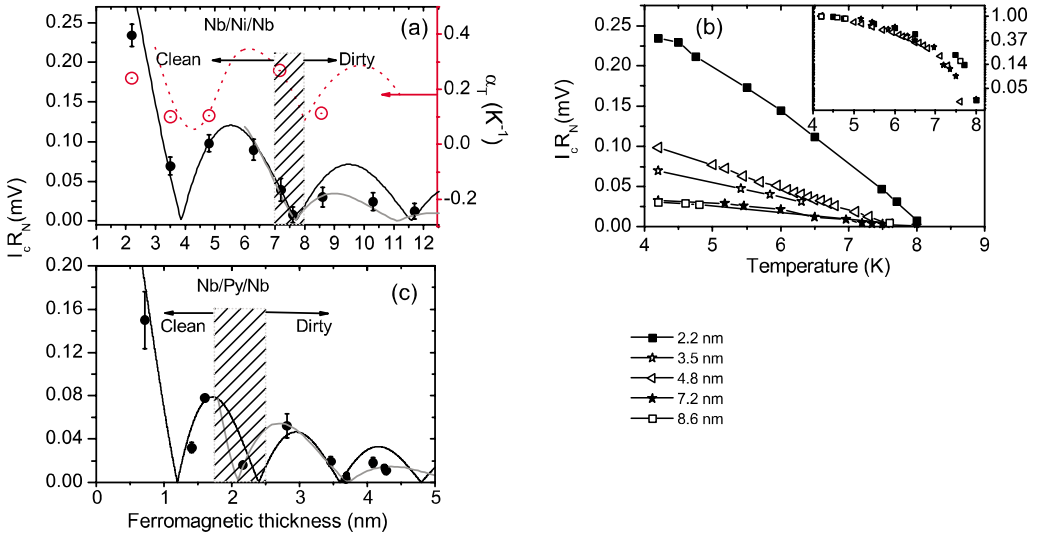

FIG. 6. (Color online) [(a) and (b)] Data for Ni barrier devices: (a) I_cR_N and α_T versus Ni thickness at 4.2 K (red dotted line is an eye guide only). (b) I_cR_N versus temperature and the inset is $I_cR_N(T)/I_cR_N$ (4.2 K) versus temperature for various devices. (c) I_cR_N versus Py thickness at 4.2 K. The black and gray curves in (a) and (c) are fits to Eqs. (4) and (6), respectively.

been shown that Nb and Ni form a variety of phases in the solid state. Such alloying at the Nb/Ni interface will modify the transport properties across the interface.

For Ni, we also investigated the thermal variation of the characteristic voltage [see Fig. 6(d)]. The results are similar to Co; the characteristic voltage decreases to 0 V in an almost monotonic fashion. Also, α_T shows an oscillatory dependence with Ni barrier thickness which, like Co, is in phase with the characteristic voltage. No critical current was observed beyond 7.8 K although there was some reduction of the differential resistance around the zero bias until 8.5 K. For $T>8.5$ K, an Ohmic like behavior was observed.

Finally, we have looked at the effect of a magnetic field on the maximum supercurrent I_{max} in our devices. We find that I_{max} oscillates with applied magnetic field, giving rise to a Fraunhofer pattern; however, we also find that I_{max}, which normally corresponds to the central peak of a Fraunhofer pattern, is offset from zero applied field to $\pm H_{offset}$, which is equal to ±4.9 mT. The inset of Fig. 5(c) shows a typical Fraunhofer pattern for an Fe barrier device with a barrier thickness of ≈2.5 nm. We compared the variation of I_{max} with applied field to the magnetic hysteresis loop of the same film (measured prior to patterning and device fabrication) at 20 K. The offset field is found to correspond approximately to the coercive field of the unpatterned film, which is $\pm H_{coercive} \simeq 4.3$ mT. The central peak is shifted by the coercive field in each direction, which is due to the changing magnetization of the ferromagnetic barrier. The side peaks are not hysteretic and displaced by the saturation moment of the barrier because the hysteresis loop is saturated and the barrier moment is constant for both field sweep directions. The coercive field and offset field in the Fraunhofer pattern do not exactly agree: firstly, the coercive field is approximated at 20 K; secondly, processing a device in a FIB microscope is likely to harden the Fe magnetic domains by virtue of Ga ion implantation. Similar results were measured for Co, Ni, and Py.

V. FERROMAGNETIC EXCHANGE ENERGY

In Sec. IV, we have estimated E_{ex} of Ni, Co, Fe, and Py to be 80 meV for Ni, 309 meV for Co, 256 meV for Fe, and 200 meV for Py. All such values are close to those reported in similar systems elsewhere, with the exception of Ni. The low value of E_{ex} for Ni could be a result of sever alloying at interface; however, further studies involving high resolution microscopy must be undertaken to confirm this. To confirm the validity of E_{ex} for Ni derived in Sec. IV, we have attempted to calculate it from its T_Θ value of 571 K, as estimated in Sec. III; however, deriving E_{ex} as a function of T_Θ is revealed to be a nontrivial problem. A T_Θ value of 571 K is in agreement with the measurement of Kim *et al.* in S/Ni bilayers[38] but is slightly below the value expected for bulk Ni films, as measured by Stanley[39] (627.2 K). If we assume $E_{ex}=2k_BT_\Theta$, then $E_{ex}=100$ meV, which is in agrement with the value we derived in Sec. IV; however, if we assume $E_{ex}=k_BT_\Theta$, then $E_{ex}=50$ meV, which is now in agreement with the estimation by Kim *et al.* of E_{ex} with S/Ni bilayer measurements. It would seem, therefore, that for our Ni, E_{ex} is "appropriately" given by $E_{ex}=2k_BT_\Theta$, which is confirmed by two measurements.

We can see, therefore, from literature that there exists a discrepancy over the relationship of E_{ex} derived from this type of measurement and T_Θ from magnetization slopes. In fact, there are two types of S/FM experiments which yield E_{ex} as a fitting parameter: (1) junctions, in which case the measured parameter is the critical current oscillation period; (2) S/FM bilayers, in which case it is the modulation of the critical current with the superconducting transition temperature. Magnetic data from these type of experiments are summarized in Fig. 7, where substantial scatter on a plot of E_{ex} vs bulk T_Θ for various ferromagnetic metals in S/FM and S/FM/S systems is shown. [40–44] To compare the relation of E_{ex} to bulk T_Θ, we have expressed both quantities in kelvin units where 1 meV≡11.645 K. Strikingly, for some S/FM bilayers, there is a good linear relationship between E_{ex} and T_Θ and the constant of proportionality is close to 1 so that $E_{ex}=k_BT_\Theta$; in contrast, all the junction data (S/FM/S) lie well above this line and there is a great deal of scatter. For the junctions, the constant of proportionality is as low as 1.2 for Fe and as high as 3.0 for CoFe. There are considerable discrepancies even where essentially the same material has been used; Ni shows an E_{ex}/T_Θ in the 0.96–3.68 range, for example. Kim *et al.*[38] used the relationship $E_{ex}=k_BT_\Theta$, and they showed that their data are consistent with this. However, we can see from Fig. 7 that most other data lie above this direct proportionality, but well below the exchange splitting energy where it has been measured by photoemission,[46] or directly calculated.

VI. PHASE SHIFT OF π IN COBALT DEVICES

In this section, we present a study of a single transition from the 0 to π state in Co devices where the mean Co barrier thickness, averaged over a 10×5 mm^2 chip, varied linearly from 1.8 to 2.5 nm. Device processing was identical to the methods summarized in Sec. II. The Co magnetic dead layer was estimated to be 1.2 nm from Fig. 8. Although larger than the dead layer estimated for the Co barriers in Sec. III of 0.8 nm, we do find from the bottom-right inset of Fig. 8 that the bulk magnetizations for the two sample sets are similar. Importantly, the magnetic data convincingly show incremental increases in magnetic moment with increasing Co thickness.

From current-voltage measurements, I_c and R_N were extracted so that I_cR_N could be determined and tracked as a function of the mean Co barrier thickness [Fig. 9(a)]. The characteristic voltage decreases to a small voltage around a mean Co barrier thickness of 2.05 nm and then increases, implying a change in phase of π. Each datum point is for each device measured, and the vertical error bars are derived from a combination of estimating I_c and R_N from the current-voltage curves and from a small noise contribution from the current source. Particularly for those devices with the smallest characteristic voltage, there is a considerable scatter in the I_cR_N values obtained. For an eye guide only, we have modeled the transition with Eq. (4), assuming E_{ex}(Co) =309 meV. The curve is offset to fit the experimental data.

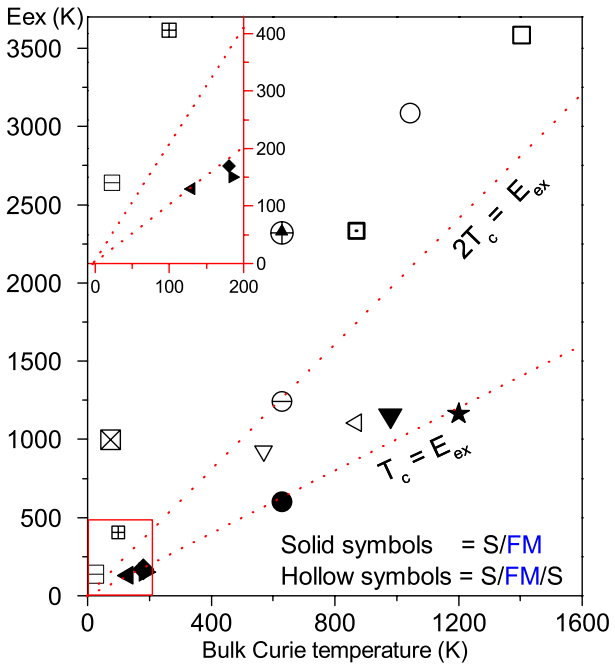

Ferromagnetic metal	Symbol	S / FM	S / FM / S	E_{ex}/T_{Curie}^{Bulk}	Ref.
Co	□	…	√	2.55	15
CoFe	★	√	…	0.97	40
$Co_{60}Fe_{40}$	▼	√	…	1.18	38
Fe	○	…	√	2.96	41
Ni	▲	√	…	3.68	42
Ni	•	√	…	0.96	38
Ni	⊕	…	√	3.68	9
Ni	⊖	…	√	3.68	34
Ni	▽	…	√	1.63	15
$Ni_{80}Fe_{20}$	⊡	…	√	2.68	15
$Ni_{80}Fe_{20}$	◁	…	√	1.26	12
$Pd_{90}Ni_{10}$	⊞	…	√	4.05	4
PdNi	▶	√	…	0.81	43
$Cu_{43}Ni_{57}$	◀	√	…	1.00	44
$Cu_{40}Ni_{60}$	♦	√	…	0.94	38
$Cu_{52}Ni_{48}$	⊟	…	√	6.09	45
Ni_3Al	⊠	…	√	13.5	8

FIG. 7. (Color online) E_{ex} values derived from S/FM bilayer experiments and from S/FM/S junction measurements: (Top) E_{ex} versus bulk T_Θ in units of kelvin (the inset is an enlargement of the region close to the origin); (bottom) symbol key and a summary of E_{ex}/T_Θ for various S/FM systems.

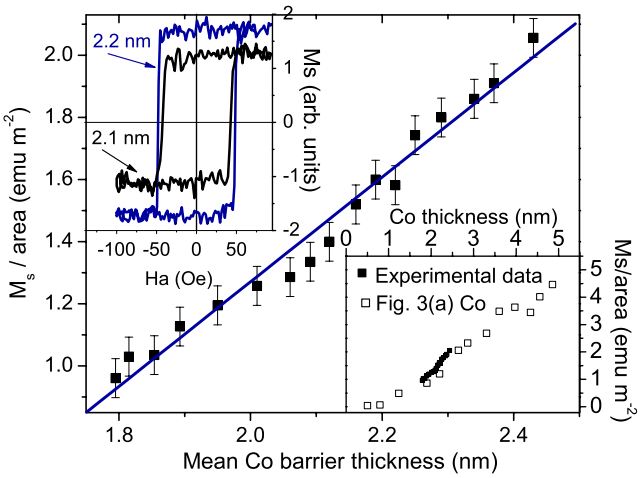

FIG. 8. (Color online) Magnetic saturation M_s per unit surface area versus mean Co thickness. Inset top left: magnetic hysteresis loops for Co thicknesses of 1.2 and 2.1 nm. Inset bottom right: a comparison of these data with the Co data in Fig. 3(a).

The model ignores any influence of a second harmonic term in the current-phase relation. In general, the current-phase relation is periodic in ϕ, the phase difference; however, recent theoretical and experimental works have looked at the possibility of observing higher order harmonics, $I_s = I_{c1}\sin\phi + I_{c2}\sin(2\phi) + \cdots$, where $I_{c2} \gg I_{c1}$ at the 0 to π crossover and the second harmonic dominates. When $I_s = I_{c2}\sin(2\phi)$, one expects both integer and half-integer Shapiro steps in the current-voltage curves at particular microwave frequencies. Until recently, no evidence for either a nonzero I_c or half-integer current steps at the transition existed. In 2004, Sellier *et al.*[45] demonstrated both a nonzero I_c at the transition and half-integer current steps; however, this was achieved in devices consisting of a weakly ferromagnetic barrier alloy of Cu and Ni where transition was controlled with temperature. In 2006, further evidence for a nonzero I_c at the transition was shown by Frolov *et al.*,[47] but again in devices consisting of a weakly ferromagnetic alloy of Cu and Ni.

The phase transition in Fig. 9(a) is not conclusive of a nonzero characteristic voltage at the transition; however, by applying microwaves in the 13–17 GHz range to those devices near the transition, we have shown that the device with the smallest characteristic voltage (chip 14, device 4) and with a Co barrier thickness of 2.1 nm exhibited current steps at both half-integer ($n=1/2$) and integer ($n=1$) values of $V/n\phi_0 f$ (f is the applied microwave frequency and ϕ_0 is the flux quantum). The current-voltage curve for chip 14 and device 4 is shown in Fig. 9(c) and compared to chip 13 and device 2 in 9(b), which only exhibited current steps at integer values of $V/n\phi_0 f$. Supporting evidence for the current steps at $n=1/2$ in chip 14 and device 4 is found from the differential resistance versus bias voltage in Fig. 9(d), where again the data are compared to chip 13 and device 2; for chip 14, device 4, the differential resistance drops abruptly at $V/n\phi_0 f = \pm 0.5$. These results imply that chip 14, device 4 is close to a minimum characteristic voltage and does provide

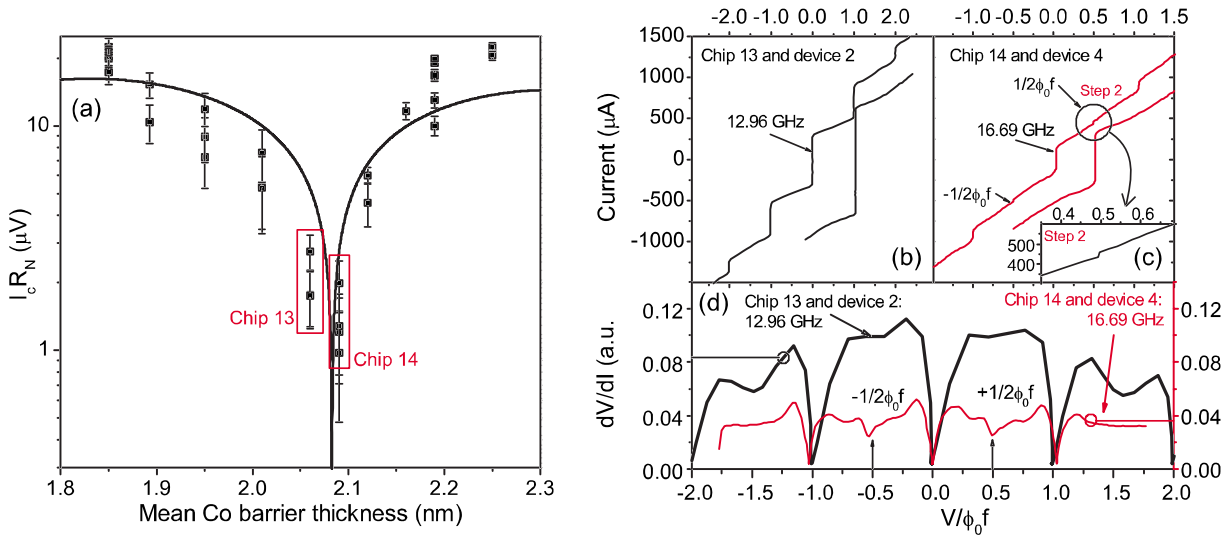

FIG. 9. (Color online) Transport properties of Nb/Co/Nb devices at 4.2 K: (a) I_cR_N versus mean Co barrier thickness compared to a fit to Eq. (4) (used as an eye guide only); (b) current-voltage curves for chip 13 and device 2 (black) without and with microwaves (12.69 GHz); (c) current-voltage curves for chip 14 and device 4 (red) without and with microwaves (16.69 GHz); (d) differential resistance across chip 13, device 2 and chip 14, device 4 versus bias voltage ($V/n\phi_0 f$). Chip 14, device 4 exhibits a sudden drop in differential resistance at $V/n\phi_0 f=0.5$. The inset of (c) shows the details of step 2 of chip 14 and device 4.

evidence for a second harmonic in the current-phase relation. Further investigations must be done before any conclusive remarks can be made.

Finally, we have estimated the electron mean free path of the Co barriers at 4.2 K. From the current-voltage characteristics of each device, we have measured the total resistance (R_N) of the unit area (A) of all of the junctions. The variation of AR_N with Co barrier thickness for $1.8<d_{Co}<2.3$ nm is shown in Fig. 10. The vertical error bars are largely derived from estimating the cross-sectional areas of the devices from a scanning electron microscope. AR_T is the total specific resistance, which is the sum of all the interfacial resistances $R_{Nb/Co}$ and $R_{Nb/Cu}$ and the layer resistances R_{Cu} and R_{Co},[48] so that

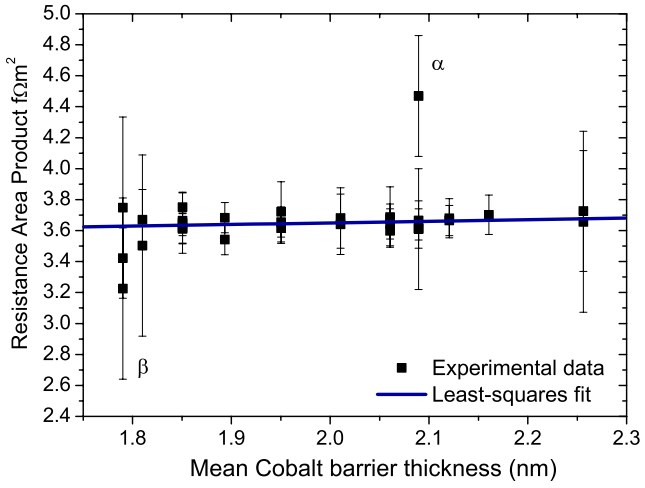

FIG. 10. (Color online) Resistance area product (AR_N) versus Co thickness at 4.2 K. The least-squares regression line ignores datum points α and β.

$$AR_T = 2[2AR_{Nb/Cu} + AR_{Nb/Co} + \rho_{Cu}d_{Cu}] + \rho_{Co}d_{Co}, \quad (8)$$

which is a straight-line equation with a gradient equal to the resistivity of the Co, $\rho_{Co}(4.2\ \mathrm{K})$. If we exclude two of the datum points with the highest AR_N products, labeled α and β, a least-squares regression line fit will have a gradient of $\rho_{Co}(4.2\ \mathrm{K}) \simeq 10(1)\times 10^{-7}\ \Omega\,\mathrm{m}$. This value is 1 order of magnitude larger than in epitaxial Co films estimated at 0 K, $\rho(0) \leqslant 1\times 10^{-6}\ \Omega\,\mathrm{m}$,[49] but similar to estimates of ρ in polycrystalline Co thin films. Assuming that the transport in Co thin films is dominated by a free-electron-like behavior, the maximum ℓ, at 0 K, may be estimated from $\ell(0) = \hbar k_F/n_e e^2\rho(0)$, where v_F is the Fermi velocity and n_e is the electron density at 0 K. Assume that $\rho(4.2)\sim\rho(0)$, $v_F=2.8\times 10^5\ \mathrm{ms}^{-1}$, and $n_e = 8\sqrt{2}\pi(mc^2)^{3/2}(2/3E_F^{3/2})/(hc)^3$, where m is the effective mass of an electron, c the speed of light in a vacuum, and E_F the Fermi energy equal to $\sqrt{1/2mv_F^2} \approx 0.224$ eV. Hence, $n_e \approx 4.81\times 10^{26}\ m^{-3}$ and $\ell(0) \approx 20.7$ nm. This provides an upper limit for ℓ at 4.2 K.

VII. SUMMARY

This paper reports a detailed systematic study of the magnetic and transport properties in the superconducting state of Nb/FM/Nb thin films consisting of the strongly ferromagnetic transition metals Co, Fe, Ni, and $Ni_{80}Fe_{20}$(Py).

The second part of the paper outlines the preparation of Nb/FM/Nb films and the subsequent processing of nanoscale vertically stacked devices. The third part discusses the magnetic properties of these films where, in particular, the scale of the magnetic dead layer within the ferromagnetic barrier is extrapolated: 0.8 nm for Co, 1.5 nm for Ni, 1.1 nm for Fe, and 0.5 nm for Py, at room temperature. From a theoretical model, the scale of the magnetic dead layer of Ni, at 4.2 K,

has been approximated to be 1.3 nm or ≈7 Å at each Nb/Ni interface. From a knowledge of the magnetic dead layer thickness, it has been shown that the magnetization of all the ferromagnets increases gradually from zero, at the edge of the dead layer zone, to a maximum value corresponding to a suppressed bulk magnetization. We attribute this reduction to interfacial factors and film quality. We conclude that although these magnetic dead layers are small, better control is needed to ensure reproducible control of the superconducting phase state.

The fourth part reports further results to support a recent publication[15] which demonstrated multiple transitions from the 0 to π states with ferromagnetic barrier thickness in Nb/FM/Nb Josephson junctions. In this section, the transport behavior of such devices in the superconducting state is reviewed, where the characteristic voltage is shown to depend on ferromagnetic thickness and temperature and where the thermal rate of decay in the characteristic voltage is also shown to depend on the ferromagnetic thickness. From existing theoretical models, the exchange energy of all the ferromagnetic metals is estimated; in doing this, an important inconsistency in the magnitude of the exchange energy derived from bilayer S/FM experiments (where exchange energy is derived from oscillations in the superconducting transition temperature) and from S/FM/S junction measurements (where the exchange energy is derived from oscillations in the critical current) compared to the bulk Curie temperatures has been uncovered (Sec. V). Results imply both interesting physics that is not currently considered in the existing theoretical models and a large inconsistency that requires a better understanding of these complex systems.

The final part, Sec. VI, reports a detailed study on the transport behavior of a single phase transition of π in Co barrier devices. Although a nonzero characteristic voltage at the transition cannot be concluded, microwave excitation measurements do provide convincing evidence for current steps at half-integer values of $V/n\phi_0 f$ for the chip and device with the smallest characteristic voltage. This strongly implies a large second harmonic in the current-phase relation.

In conclusion, the results reported in this paper can be summarized in the following notable points: (1) A better understanding of the magnetic behavior of nanoscale thick ferromagnetic films grown on other metallic systems is needed—this is critical both to the understanding of the hybridization processes of transition ferromagnets with other metallic systems and the understanding, control, and development of the superconductor-(strongly) ferromagnet proximity effect; (2) the possibility of a second harmonic in the current-phase relation in superconductor-(strongly) ferromagnet-superconductor Josephson junctions.

ACKNOWLEDGMENTS

The authors thank N. Stelmashenko for technical guidance and James Witt for experimental contributions. They also acknowledge financial support from EPSRC, UK.

[1] A. I. Buzdin, Nat. Mater. **3**, 751 (2004).
[2] A. I. Buzdin, Rev. Mod. Phys. **77**, 935 (2005).
[3] V. V. Ryazanov, V. A. Oboznov, A. Yu. Rusanov, A. V. Veretennikov, A. A. Golubov, and J. Aarts, Phys. Rev. Lett. **86**, 2427 (2001).
[4] T. Kontos, M. Aprili, J. Lesueur, F. Genêt, B. Stephanidis, and R. Boursier, Phys. Rev. Lett. **89**, 137007 (2002).
[5] L. N. Bulaevskii, V. V. Kuzii, and A. A. Sobyanin, JETP Lett. **25**, 290 (1997).
[6] A. I. Larkin and Y. N. Ovchinnokov, Sov. Phys. JETP **20**, 762 (1965).
[7] P. Fulde and R. A. Ferrell, Phys. Rev. **135**, A550 (1964).
[8] F. Born, M. Siegel, E. K. Hollmann, H. Braak, A. A. Golubov, D. Yu. Gusakova, and M. Yu. Kupriyanov, Phys. Rev. B **74**, 140501(R) (2006).
[9] V. Shelukhin, A. Tsukernik, M. Karpovski, Y. Blum, K. B. Efetov, A. F. Volkov, T. Champel, M. Eschrig, T. Lofwander, G. Schon, and A. Palevski, Phys. Rev. B **73**, 174506 (2006).
[10] A. Wallraff, D. I. Schuster, A. Blais, L. Frunzio, J. Majer, M. H. Devoret, S. M. Girvin, and R. J. Schoelkopf, Phys. Rev. Lett. **95**, 060501 (2005).
[11] M. A. Nielsen and I. L. Chuang, *Quantum Computation and Quantum Information* (Cambridge University Press, Cambridge, England, 2000).
[12] C. Bell, R. Loloee, G. Burnell, and M. G. Blamire, Phys. Rev. B **71**, 180501(R) (2005).
[13] Y. Obi, M. Ikebe, T. Kubo, and H. Fujimori, Physica C **318**, 149 (1999).
[14] J. E. Mattson, R. M. Osgood, C. D. Potter, C. H. Sowers, and S. D. Bader, J. Vac. Sci. Technol. A **15**, 1774 (1997).
[15] J. W. A Robinson, S. Piano, G. Burnell, C. Bell, and M. G. Blamire, Phys. Rev. Lett. **97**, 177003 (2006).
[16] C. Bell, R. H. Hadfield, G. Burnell, D.-J. Kang, M. J. Kappers, and M. G. Blamire, Nanotechnology **14**, 630 (2003).
[17] C. C. Kuo, W. C. Lin, C. L. Chiu, H. L. Huang, and Minn-Tsong Lin, J. Appl. Phys. **89**, 7153 (2001).
[18] F. Wilhelm, U. Bovensiepen, A. Scherz, P. Poulopoulos, A. Ney, H. Wende, G. Ceballos, and K. Baberschke, J. Magn. Magn. Mater. **222**, 163 (2000).
[19] M. Kitada and N. Shimizu, J. Mater. Sci. Lett. **10**, 437 (1991).
[20] J. Aarts, J. M. E. Geers, E. Brück, A. A. Golubov, and R. Coehoorn, Phys. Rev. B **56**, 2779 (1997).
[21] R. Zhang and R. F. Willis, Phys. Rev. Lett. **86**, 2665 (2001).
[22] S. Pick, I. Turek, and H. Dreysse, Solid State Commun. **124**, 21 (2002).
[23] Qunwen Leng, Hua Han, Ming Mao, Craig Hiner, and Francis Ryan, J. Appl. Phys. **87**, 6621 (2000).
[24] J. C. Slator, J. Appl. Phys. **8**, 385 (1937).
[25] L. Pauling, Phys. Rev. **54**, 899 (1938).
[26] Sóshin Chikazumi, *Physics of Ferromagnetism* (Oxford University Press, England, 1997).
[27] J. Lee, G. Lauhoff, S. Hope, C. Daboo, J. A. C. Bland, J. Ph. Schille, G. van der Laan, and J. Penfold, J. Appl. Phys. **81**, 3893 (1997).

[28] L. Liebermann, D. R. Fredkin, and H. B. Shore, Phys. Rev. Lett. **22**, 539 (1969).
[29] L. Liebermann, J. Clinton, D. M. Edwards, and J. Mathon, Phys. Rev. Lett. **25**, 232 (1970).
[30] Hailin Chen, Yong Du, Hongchui Xu, and Yong Liu, J. Mater. Sci. **40**, 6019 (2005).
[31] A. I. Buzdin, JETP Lett. **35**, 178 (1982).
[32] F. S. Bergeret, A. F. Volkov, and K. B. Efetov, Phys. Rev. B **64**, 134506 (2001).
[33] C. W. Leung, M. E. Vickers, J. D. R. Buchanan, and M. G. Blamire, J. Magn. Magn. Mater. **269**, 15 (2004).
[34] Y. Blum, A. Tsukernik, M. Karpovski, and A. Palevski, Phys. Rev. Lett. **89**, 187004 (2002).
[35] V. A. Oboznov, V. V. Bol'ginov, A. K. Feofanov, V. V. Ryazanov, and A. I. Buzdin, Phys. Rev. Lett. **96**, 197003 (2006).
[36] K. N. Altmann, N. Gilman, J. Hayoz, R. F. Willis, and F. J. Himpsel, Phys. Rev. Lett. **87**, 137201 (2001).
[37] Bruce A. Gurney, Virgil S. Speriosu, Jean-Pierre Nozieres, Harry Lefakis, Dennis R. Wilhoit, and Omar U. Need, Phys. Rev. Lett. **71**, 4023 (1993).
[38] J. Kim, J. H. Kwon, K. Char, H. Doh, and H. Y. Choi, Phys. Rev. B **72**, 014518 (2005).
[39] C. Kittel, *Introduction to Solid State Physics* (Wiley, New York, 1996).
[40] S. Reymond, P. SanGiorgio, M. R. Beasley, J. Kim, T. Kim, and K. Char, Phys. Rev. B **73**, 054505 (2006).
[41] S. Piano, J. W. A Robinson, G. Burnell, and M. G. Blamire, Eur. Phys. J. B **58**, 123 (2007).
[42] A. S. Sidorenko, V. I. Zdravkov, A. A. Prepelitsa, C. Hebig, Y. Luo, S. Gsell, M. Schreck, S. Klimm, S. Horn, L. R. Tagriov, and R. Tidocks, Ann. Phys. (N.Y.) **12**, 37 (2003).
[43] C. Cirillo, S. L. Prischepa, M. Salvato, C. Attanasio, M. Hesselberth, and J. Aarts, Phys. Rev. B **72**, 144511 (2005).
[44] Ya. V. Fominov, N. M. Chtchelkatchev, and A. A. Golubov, Phys. Rev. B **66**, 014507 (2002).
[45] H. Sellier, C. Baraduc, F. Lefloch, and R. Calemczuk, Phys. Rev. Lett. **92**, 257005 (2004).
[46] P. Heinmann, F. J. Himpsel, and D. E. Eastman, Solid State Commun. **39**, 219 (1981).
[47] S. M. Frolov, D. J. Van Harlingen, V. V. Bolginov, V. A. Oboznov, and V. V. Ryazanov, Phys. Rev. B **74**, 020503(R) (2006).
[48] Q. Yang, P. Holody, R. Loloee, L. L. Henry, W. P. Pratt, Jr., P. A. Schroeder, and J. Bass, Phys. Rev. B **51**, 3226 (1995).
[49] U. Rüdiger, J. Yu, L. Thomas, S. S. P. Parkin, and A. D. Kent, Phys. Rev. B **59**, 11914 (1999).